

Thermal boundary resistance predictions with non-equilibrium Green's function and molecular dynamics simulations

Cite as: Appl. Phys. Lett. **115**, 231601 (2019); doi: [10.1063/1.5125037](https://doi.org/10.1063/1.5125037)

Submitted: 20 August 2019 · Accepted: 18 November 2019 ·

Published Online: 2 December 2019








View Online



Export Citation



CrossMark

Yuanchen Chu,^{1,a),b)}  Jingjing Shi,^{2,a)}  Kai Miao,¹ Yang Zhong,²  Prasad Sarangapani,¹  Timothy S. Fisher,³ 
Gerhard Klimeck,^{1,4,5}  Xiulin Ruan,²  and Tillmann Kubis^{1,4,5,6} 

AFFILIATIONS

¹School of Electrical and Computer Engineering, Purdue University, West Lafayette, Indiana 47907, USA

²School of Mechanical Engineering, Purdue University, West Lafayette, Indiana 47907, USA

³Department of Mechanical and Aerospace Engineering, University of California, Los Angeles, California 90095, USA

⁴Network for Computational Nanotechnology, Purdue University, West Lafayette, Indiana 47907, USA

⁵Purdue Center for Predictive Materials and Devices, West Lafayette, Indiana 47907, USA

⁶Purdue Institute of Inflammation, Immunology and Infectious Disease, West Lafayette, Indiana 47907, USA

^{a)}Contributions: Y. Chu and J. Shi contributed equally to this work.

^{b)}Email: chu72@purdue.edu

ABSTRACT

The nonequilibrium Green's function (NEGF) method with Büttiker probe scattering self-energies is assessed by comparing its predictions for the thermal boundary resistance with molecular dynamics (MD) simulations. For simplicity, the interface of Si/heavy-Si is considered, where heavy-Si differs from Si only in the mass value. With Büttiker probe scattering parameters tuned against MD in homogeneous Si, the NEGF-predicted thermal boundary resistance quantitatively agrees with MD for wide mass ratios. Artificial resistances that the unaltered Landauer approach yields at virtual interfaces in homogeneous systems are absent in the present NEGF approach. Spectral information results from NEGF in its natural representation without further transformations. The spectral results show that the scattering between different phonon modes plays a crucial role in thermal transport across interfaces. Büttiker probes provide an efficient and reliable way to include anharmonicity in phonon related NEGF. NEGF including the Büttiker probes can reliably predict phonon transport across interfaces and at finite temperatures.

Published under license by AIP Publishing. <https://doi.org/10.1063/1.5125037>

Semiconductor nanodevices such as quantum cascade lasers, light-emitting diodes, and thermoelectric devices are typically composed of several semiconductor materials.^{1–4} Scattering of thermal energy carriers at the interface between two materials results in thermal boundary resistance.⁵ The size of the thermal boundary resistance was previously reported⁶ to be comparable to that of pure materials with lengths of a few to tens of nanometers. Predicting the thermal boundary resistance gives important insight into the device physics and enables design improvements. Often, molecular dynamics (MD) is used to model the thermal boundary resistance and reproduce experimental data.⁷ Inelastic phonon scattering is included in MD simulations through the anharmonicity of the interatomic potential.⁸ The nonequilibrium Green's function (NEGF) method⁹ is widely

accepted as one of the most consistent methods for electronic quantum transport in nanodevices.^{10,11} In particular, for predicting stationary device physics, NEGF is potentially more attractive than MD, given that it is a spectral approach when setup in energy space, though modal methods in nonequilibrium MD have just begun to be developed.^{12,13} When electrons and phonons are both solved in the NEGF framework, interparticle interactions and energy and momentum transfer in, e.g., self-heating or thermoelectric situations can be described on equal footing with the predictions of the respective particles' propagation.¹⁴ For phonon transport, however, the NEGF method has been used predominantly in the coherent (harmonic) regime due to the fact that the inclusion of incoherent scattering such as phonon-phonon decay usually requires solving polarization graphs

in the self-consistent Born approximation, which entails a large numerical load.¹⁵ It has been shown that the lack of anharmonicity in NEGF simulation gives incorrect thermal boundary resistance predictions at high temperatures.^{16–18}

In this work, a numerically efficient method to solve phonon transport in the NEGF framework including phenomenological phonon scattering with Büttiker probes is presented and benchmarked against MD. The artificial resistance at the virtual interface in a homogeneous structure that plagues the equilibrium Landauer approach^{6,19} is absent in the presented NEGF approach. When solved for homogeneous systems, this NEGF method yields vanishing interface resistance. The thermal boundary resistance calculated with this NEGF method shows quantitative agreement with MD simulations. The extracted spectral transport information from NEGF shows that the different phonon modal contributions play an important role in thermal transport across the interface.

Figure 1(a) shows the simulation domain considered in both MD and NEGF. The system consists of Si to the left and heavy-Si to the right of an interface at position 0. The heavy-Si differs from Si only in its atomic mass ratio vs Si $MR = M_{hSi}/M_{Si}$. For all simulations in this work, M_{Si} is fixed at 28.085 u and a range of 1 to 10 is considered for MR . Transport is solved within a range $L/2$ to the left and right of the interface. The lattice temperature for regions further to the left and right of the interface is assumed to be constant and equal to 320 K and 280 K, respectively. Phonon transport occurs along the x direction, and the system is considered to be periodic along y and z directions. The harmonic phonon band structure is described with a Tersoff potential,²⁰ and the lattice constant is set to 5.431 Å. The details of the thermal boundary resistance extraction are illustrated in Fig. 1(b). First, linear fits are performed on the local temperature profiles to the left and the right of the interface, respectively. The local temperature T is obtained by minimizing the difference between the local phonon energy density and the product of a local Bose-Einstein distribution and the local phonon density of states (LDOS).²¹ For a given atom, the local temperature T solves the equation

$$\sum_{q_{\parallel}} \int_0^{\infty} \omega \rho(\omega) d\omega = \sum_{q_{\parallel}} \int_0^{\infty} \omega D(\omega) f_{BE}(\omega, T) d\omega, \quad (1)$$

where ω is the phonon frequency and q_{\parallel} is the transverse phonon wave vector. ρ is the local phonon number density and D is the local phonon density of states. The temperatures T_1 and T_2 of the Si and heavy Si in the vicinity of the interface [see Fig. 1(b)] are determined with the fitted temperature profiles. Finally, the thermal boundary resistance is calculated as $R = (T_1 - T_2)/q$, where q is the simulated heat flux. Following the discussion in Ref. 22, three different device lengths L are simulated for each value of MR , and R is extracted for the limit of $1/L = 0$ by linear extrapolation.

The LAMMPS package²³ is used for all MD simulations in this work. The lengths of both the heat source and the heat sink are $L/10$, and the simulation time step is 0.4 fs. Periodic boundary conditions are applied in y and z directions, while the fixed boundary condition²⁴ is applied in the x direction. For MD calculations, the discretized device cross section is of 8×8 conventional unit cells, with each conventional cell containing 8 atoms. First, a canonical ensemble (NVT) is considered and run for 1.2 ns to relax the structure, allowing the system to reach thermal equilibrium at 300 K. The system is then switched to a microcanonical ensemble (NVE), and a constant heat flux is added to the heat source and extracted from the heat sink for 12 ns. After the system reaches the steady state, the local temperature of each cell is obtained by averaging over ten million timesteps in the last 4 ns. L of 92, 130, and 184 unit cells is used for MD based simulation of each MR value.

For all NEGF simulations, the nanodevice simulation tool NEMO5²⁵ is used. Stationary Green's functions are solved in the energy domain, which gives spectral data without additional transformations. To calculate the harmonic interatomic force constants (IFCs), a $3 \times 3 \times 3$ unit cell bulk Si structure is relaxed in LAMMPS using the Tersoff potential.²⁰ The derivatives of the forces between atoms with respect to the atom position variations give the harmonic IFCs. These values are then loaded into NEMO5 to construct the dynamical matrix.²⁶ Only the transport direction (x) is discretized in real space. The periodic directions (y and z) are represented with a single conventional unit cell. Longer-ranged periodicity is represented with the phonon momenta in reciprocal space. Anharmonic phonon decay is included via Büttiker probes.²⁷ The Büttiker probe self-energies at atom i with vibrational direction $m(x, y, z)$ are of the form

$$\Sigma_{BP(i,m)}^R(\omega) = -i \frac{2\omega\hbar^2}{\tau_{(i,m)}(\omega)}. \quad (2)$$

Each discretized atom in the system has a Büttiker probe applied to it. Following Ref. 21, we approximate the phonon frequency (ω) dependent scattering lifetime τ as isotropic and assume it represents only the phonon-phonon Umklapp process,²⁸

$$\tau_{(i,m)}^{-1}(\omega) = \tau_i^{-1}(\omega) = BT_i\omega^2 e^{-C/T_i}. \quad (3)$$

T_i is the phonon Büttiker probe temperature of the atom i . It represents the local temperature for the limit of complete phonon thermalization at each atom. The actual local temperature differs from the Büttiker probe one depending on the scattering strength.²⁸ To ensure energy conservation, the Büttiker probe temperature is solved iteratively by Newton's method until the integrated energy current vanishes

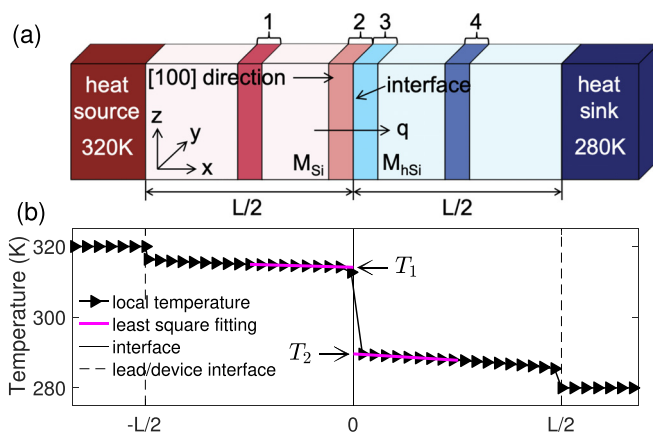


FIG. 1. (a) Simulation domain considered in this work. Regions marked by 1 through 4 are three atomic layers in the middle of Si, left to the interface, right to the interface, and in the middle of heavy Si, respectively. (b) Schematic of the thermal boundary resistance extraction.

for each Büttiker probe.²¹ Since the phonon Green's functions are solved with the recursive Green's function (RGF) method,²¹ the device is partitioned into slabs perpendicular to the transport direction. This limits the peak memory usage during computation but requires the Büttiker probe self-energies to be equal throughout each slab. The parameters B (5×10^{-20} s/K) and C (430 K) are chosen such that the NEGF prediction of the bulk Si thermal conductivity agrees with the MD solution [see Fig. 2(a)]. The same values of B and C are used in Si and heavy-Si. In this way, the dependence of the scattering rate on the atomic mass and deviations of the anharmonicity near the interface from the one of the volume materials are ignored. This is not a fundamental limitation of the Büttiker probes. Future work on other materials and interfaces might likely require a more detailed Büttiker probe model. L of 146, 184, and 220 unit cells is used for NEGF based simulation of each MR value.

The spatial distribution of local phonon density of states (LDOS) can illustrate the contributions of different phonon modes to the heat flux in various regions. For this purpose, four regions of interest, consisting of three atomic layers each, are defined in Fig. 1(a). The LDOS $\phi_i(\omega)$ of any region i of these regions is averaged over all of its atoms. For a given phonon frequency, the L1-norm of the LDOS summed over all regions is defined as

$$\|\phi_{tot}(\omega)\| = \sum_{i=1}^4 \phi_i(\omega). \quad (4)$$

The relative contribution of LDOS of region i is then defined as

$$R_i(\omega) = \frac{\phi_i(\omega)}{\|\phi_{tot}(\omega)\|}. \quad (5)$$

Figure 2(b) shows that the thermal boundary resistance as a function of MR calculated with NEGF agrees quantitatively with the MD predictions. For both methods, the thermal boundary resistance increases

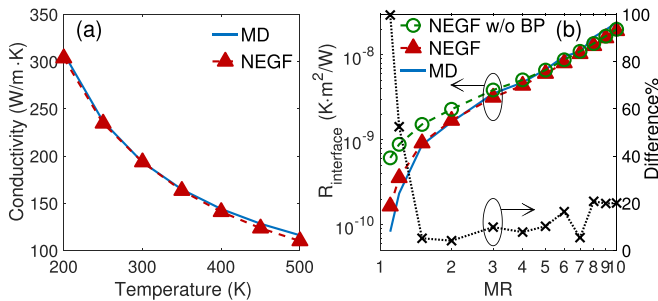


FIG. 2. (a) Thermal conductivity of bulk Si calculated with MD and NEGF. The Büttiker probe parameters B and C are fitted such that the transport results of NEGF agree with MD. (b) Thermal boundary resistance as a function of the mass ratio (MR) calculated by NEGF with the fitted parameters B and C of (a) and MD. The error bar of MD simulation is calculated but not plotted since the standard deviation for independent simulations is only 1.6% to 4.6% of the average resistance at the Si/heavy-Si interface for different mass ratios. The dotted line is the relative difference of the two methods and is defined as $(NEGF - MD)/MD \times 100\%$. The green curve shows the results calculated by NEGF without Büttiker probe self-energies. With increasing masses, the maximum phonon frequency and [with the frequency dependence of the Büttiker probes, Eq. (2)] the average scattering strength reduce. Consequently, the impact of scattering on $R_{interface}$ declines with increasing mass of heavy-Si.

exponentially with MR and vanishes when MR tends to unity (i.e., for a homogeneous system). The small remaining difference between the MD and NEGF results is systemic to the different treatment of phonon modes perpendicular to the transport direction: in NEGF, the phonon momentum perpendicular to transport is explicitly resolved as a parameter in the Dyson and Keldysh equations.²¹ In contrast, MD calculations require as large as possible unit cells perpendicular to transport to cover as many phonon modes with long wavelengths in these directions as feasible. Another source of differences can be the open boundary condition in the transport direction: Figs. 3(a) and 3(b) benchmark the open boundary condition treatment in MD and NEGF, since they illustrate finite-size effects⁷ with the thermal boundary resistance R as a function of the inverse system length $1/L$. For MD, the slope of R vs $1/L$ increases with the mass ratio MR , i.e., with reducing average sound velocity in the device. This agrees with similar findings discussed in detail in Ref. 7. Note that the mean free path of Si at room temperature is about 300 nm.²⁹ Therefore, it is practically impossible to completely eliminate the size effect along the transport direction in MD due to computational cost. In contrast to the finite sized boundary reservoirs of MD, contact self-energies in NEGF incorporate semi-infinite leads as phonon reservoirs.³⁰ Accordingly, we observe the slope of R vs $1/L$ in NEGF predictions is much smaller than that of MD. Also, its increase with MR is comparably negligible. This different boundary treatment is another source of some differences between MD and NEGF seen in Fig. 2(b).

Figure 4(a) shows the phonon density of states (DOS) in homogeneous Si and heavy-Si solved with NEGF. The DOS of heavy-Si is limited to energies at or below 33.3 meV, two times less than in native Si in agreement with the applied $MR=4$. Incoherent phonon scattering allows phonons with energies above this heavy-Si cutoff energy to propagate. This is illustrated in Figs. 4(b)–4(d) with the energy resolved current densities of the heat source and heat sink of the device in Fig. 1(a) when solved in NEGF with different scattering strengths. While the energy distribution changes with scattering, the total energy current (on the order of 10^9 W/m²) is conserved, and the difference of the total energy current between the source and the sink is on the order of 1 W/m². In Fig. 4(b), normal scattering strength (fitted to reproduce the MD-calculated bulk thermal conductivity) is applied.

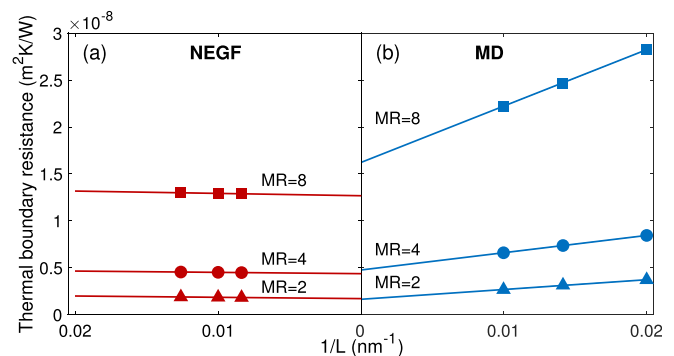


FIG. 3. Linear extrapolation of (a) NEGF and (b) MD for three MR values. MD results show a stronger dependence on the length of the device. Open boundary conditions included in NEGF with contact self-energies give almost device size independent results.

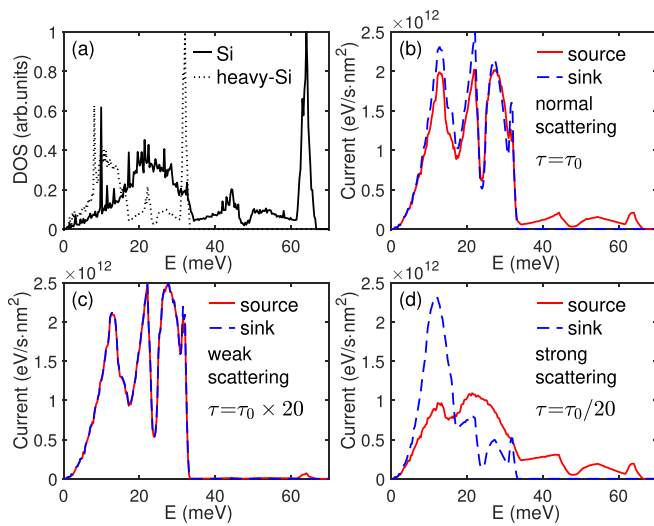


FIG. 4. (a) Energy resolved (transverse momentum integrated) density of states in Si and heavy-Si leads. (b)–(d) Energy resolved (transverse momentum integrated) current of NEGF in the heat source and sink calculated with normal, artificially weak ($1/20\times$), and artificially strong ($20\times$) scattering strengths, respectively.

The source current with energies above the energy cutoff is finite since its corresponding phonons can relax to lower energies at the heavy-Si side via inelastic scattering. In Fig. 4(c), an artificially weak scattering strength is used ($1/20\times$ normal scattering strength). Accordingly, the profiles of current in both the heat source and sink follow the profile of the heavy-Si DOS. In contrast, Fig. 4(d) shows the NEGF results when artificially strong scattering is used ($20\times$ normal scattering strength). The current profiles in the heat source and heat sink follow the profiles of the DOS in the Si and the heavy-Si leads, respectively. The results show that stronger inelastic scattering brings the system closer to local thermodynamic equilibrium.

In Fig. 4(b), four current peaks in the heavy-Si heat sink are located at 12 meV, 22 meV, 27 meV, and 32 meV, respectively. They correspond to the four peaks of the heavy-Si DOS shown in Fig. 4(a). The relative magnitudes of the four current peaks do not follow the relative magnitudes of the four DOS peaks (i.e., the list of current peaks arranged in decreasing order of magnitude is $22\text{ meV} > 12\text{ meV} > 27\text{ meV} > 32\text{ meV}$, whereas the same list according to the DOS magnitude is $32\text{ meV} > 12\text{ meV} > 22\text{ meV} > 27\text{ meV}$). Without interfaces involved, the current is expected to be proportional to the product of the DOS and the group velocity.³¹ The results of Fig. 4 can be understood in Fig. 5, since it illustrates the different relative contributions of phonon modes in different device areas. Phonon modes around 12 meV reside nearly exclusively in the heavy-Si. Consequently, they contribute less to the overall heat current. In contrast, phonon modes around 22 meV are present in all 4 device regions considered in Fig. 5. Therefore, these modes can maintain a higher contribution to the total heat current.

In conclusion, NEGF with Büttiker probe scattering is applied to the thermal boundary resistance of the Si/heavy-Si interface. The empirical NEGF scattering parameters are tuned to reproduce the thermal conductivity of homogeneous Si predicted by MD. The scattering parameters proved to be transferable, since the NEGF results of

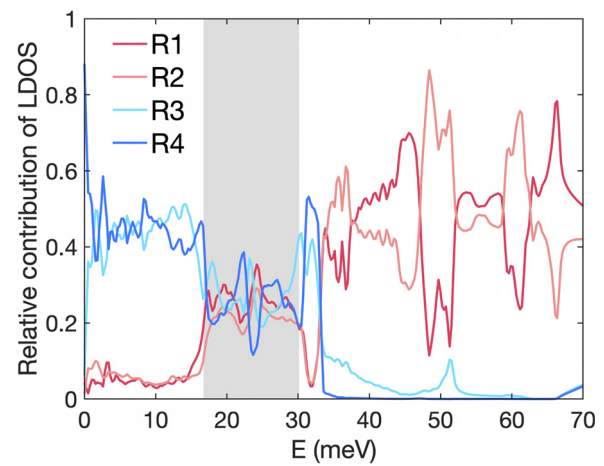


FIG. 5. The ratio of the phonon mode in regions 1–4 defined in Fig. 1 and by Eq. (4) ($\sum_{i=1}^4 R_i = 1$). The evenly distributed phonon modes around 22 meV (marked by the gray area) result in the highest current peak at 22 meV [see Fig. 4(b)] although having a lower DOS and lower group velocity compared to those at 12 meV.

the thermal boundary resistance quantitatively agree with MD results for mass ratios ranging from 1 to 10. The artificial resistance at the virtual interface in a homogeneous structure that plagues the equilibrium Landauer approach is absent in the presented NEGF approach. Besides, the present NEGF approach is found to be numerically more efficient than MD. Thanks to the open boundary conditions, NEGF shows virtually no finite-size effects compared to MD. The analysis of the NEGF spectral information shows that the scattering between different phonon modes determines the phonon energy current flow across interfaces. Future improvements of our approach can include a more accurate description of inelastic scattering at the interface and enable the computationally efficient calculation of spectral current adjacent to the interface.

Tillmann Kubis acknowledges support from Silvaco, Inc. Jingjing Shi, Timothy Fisher, and Xiulin Ruan would like to acknowledge the support from the Air Force Office of Scientific Research (AFOSR) MURI Grant (No. FA9550-12-1-0037). This research was supported in part through computational resources provided by Information Technology at Purdue, West Lafayette, Indiana. This research is part of the Blue Waters sustained-petascale computing project, which is supported by the National Science Foundation (Award No. ACI 1238993) and the state of Illinois. Blue Waters is a joint effort of the University of Illinois at Urbana-Champaign and its National Center for Supercomputing Applications.

REFERENCES

- ¹Z. I. Alferov, “The history and future of semiconductor heterostructures,” *Semiconductors* **32**, 1–14 (1998); e-print [arXiv:1011.1669v3](https://arxiv.org/abs/1011.1669v3).
- ²J. Faist, F. Capasso, D. L. Sivco, C. Sirtori, A. L. Hutchinson, and A. Y. Cho, “Quantum cascade laser,” *Science* **264**, 553–556 (1994).
- ³S. Nakamura, T. Mukai, and M. Senoh, “Candela-class high-brightness InGaN/AlGaIn double-heterostructure blue-light-emitting diodes,” *Appl. Phys. Lett.* **64**, 1687–1689 (1994); e-print [arXiv:1011.1669v3](https://arxiv.org/abs/1011.1669v3).

- ⁴M. L. Tsai, S. H. Su, J. K. Chang, D. S. Tsai, C. H. Chen, C. I. Wu, L. J. Li, L. J. Chen, and J. H. He, "Monolayer MoS₂ heterojunction solar cells," *ACS Nano* **8**, 8317–8322 (2014); e-print [arXiv:1408.1149](https://arxiv.org/abs/1408.1149).
- ⁵E. T. Swartz and R. O. Pohl, "Thermal boundary resistance," *Rev. Mod. Phys.* **61**, 605–668 (1989).
- ⁶E. S. Landry and A. J. H. McGaughey, "Thermal boundary resistance predictions from molecular dynamics simulations and theoretical calculations," *Phys. Rev. B* **80**, 165304 (2009).
- ⁷P. K. Schelling, S. R. Phillpot, and P. Keblinski, "Comparison of atomic-level simulation methods for computing thermal conductivity," *Phys. Rev. B* **65**, 1–12 (2002).
- ⁸P. E. Hopkins, "Multiple phonon processes contributing to inelastic scattering during thermal boundary conductance at solid interfaces," *J. Appl. Phys.* **106**, 013528 (2009).
- ⁹S. Datta, "Nanoscale device modeling: The Green's function method," *Superlattices Microstruct.* **28**, 253–278 (2000).
- ¹⁰J. Knoch, S. Mantl, and J. Appenzeller, "Impact of the dimensionality on the performance of tunneling FETs: Bulk versus one-dimensional devices," *Solid-State Electron.* **51**, 572–578 (2007).
- ¹¹A. Mátyás, T. Kubis, P. Lugli, and C. Jirauschek, "Comparison between semiclassical and full quantum transport analysis of THz quantum cascade lasers," *Physica E* **42**, 2628–2631 (2010).
- ¹²K. Sääskilähti, J. Oksanen, J. Tulkki, and S. Volz, "Role of anharmonic phonon scattering in the spectrally decomposed thermal conductance at planar interfaces," *Phys. Rev. B* **90**, 134312 (2014).
- ¹³T. Feng, W. Yao, Z. Wang, J. Shi, C. Li, B. Cao, and X. Ruan, "Spectral analysis of nonequilibrium molecular dynamics: Spectral phonon temperature and local nonequilibrium in thin films and across interfaces," *Phys. Rev. B* **95**, 195202 (2017).
- ¹⁴C. Stieger, A. Szabo, T. Bunjako, and M. Luisier, "*Ab-initio* quantum transport simulation of self-heating in single-layer 2-D materials *Ab-initio* quantum transport simulation of self-heating in single-layer 2-D materials," *J. Appl. Phys.* **122**, 045708 (2017).
- ¹⁵M. Luisier, "Atomistic modeling of anharmonic phonon-phonon scattering in nanowires," *Phys. Rev. B* **86**, 245407 (2012).
- ¹⁶J. T. Gaskins, G. Kotsonis, A. Giri, S. Ju, A. Rohskopf, Y. Wang, T. Bai, E. Sachet, C. T. Shelton, Z. Liu, Z. Cheng, B. M. Foley, S. Graham, T. Luo, A. Henry, M. S. Goorsky, J. Shiomi, J. P. Maria, and P. E. Hopkins, "Thermal boundary conductance across heteroepitaxial ZnO/GaN interfaces: Assessment of the phonon gas model," *Nano Lett.* **18**, 7469–7477 (2018).
- ¹⁷C. A. Polanco, R. Rastgarkafshgarkolaei, J. Zhang, N. Q. Le, P. M. Norris, and A. W. Ghosh, "Design rules for interfacial thermal conductance: Building better bridges," *Phys. Rev. B* **95**, 195303 (2017).
- ¹⁸N. Q. Le, C. A. Polanco, R. Rastgarkafshgarkolaei, J. Zhang, A. W. Ghosh, and P. M. Norris, "Effects of bulk and interfacial anharmonicity on thermal conductance at solid/solid interfaces," *Phys. Rev. B* **95**, 245417 (2017).
- ¹⁹J. Shi, X. Yang, T. S. Fisher, and X. Ruan, "Dramatic increase in the thermal boundary conductance and radiation limit from a nonequilibrium Landauer approach," preprint [arXiv:1812.07910](https://arxiv.org/abs/1812.07910) (2018).
- ²⁰J. Tersoff, "Modeling solid-state chemistry: Interatomic potentials for multi-component systems," *Phys. Rev. B* **39**, 5566–5568 (1989).
- ²¹S. Sadasivam, N. Ye, J. P. Feser, J. Charles, K. Miao, T. Kubis, and T. S. Fisher, "Thermal transport across metal silicide-silicon interfaces: First-principles calculations and Green's function transport simulations," *Phys. Rev. B* **95**, 085310 (2017).
- ²²D. Sellan, E. Landry, J. Turney, A. McGaughey, and C. Amon, "Size effects in molecular dynamics thermal conductivity predictions," *Phys. Rev. B* **81**, 1–10 (2010).
- ²³S. Plimpton, "Fast parallel algorithms for short-range molecular dynamics," *J. Comput. Phys.* **117**(1), 1–19 (1995).
- ²⁴B. J. Alder and T. E. Wainwright, "Studies in molecular dynamics. I. General method," *J. Chem. Phys.* **31**, 459–466 (1959).
- ²⁵S. Steiger, M. Povolotskiy, H. H. Park, T. Kubis, and G. Klimeck, "Nemo5: A parallel multiscale nanoelectronics modeling tool," *IEEE Trans. Nanotechnol.* **10**, 1464–1474 (2011).
- ²⁶A. Paul, M. Luisier, and G. Klimeck, *J. Comput. Electron.* **9**, 160–172 (2010).
- ²⁷M. Büttiker, "Four-terminal phase-coherent conductance," *Phys. Rev. Lett.* **57**, 1761–1764 (1986).
- ²⁸K. Miao, S. Sadasivam, J. Charles, G. Klimeck, T. S. Fisher, and T. Kubis, "Büttiker probes for dissipative phonon quantum transport in semiconductor nanostructures," *Appl. Phys. Lett.* **108**, 113107 (2016).
- ²⁹Y. S. Ju and K. E. Goodson, "Phonon scattering in silicon films with thickness of order 100 nm," *Appl. Phys. Lett.* **74**, 3005–3007 (1999).
- ³⁰S. Datta, *Quantum Transport: Atom to Transistor* (Cambridge University Press, 2005).
- ³¹S. Datta, *Electronic Transport in Mesoscopic Systems*, Cambridge Studies in Semiconductor Physics and Microelectronic Engineering (Cambridge University Press, 1995).